RSC Advances

ROYAL SOCIETY OF CHEMISTRY

www.rsc.org/advances

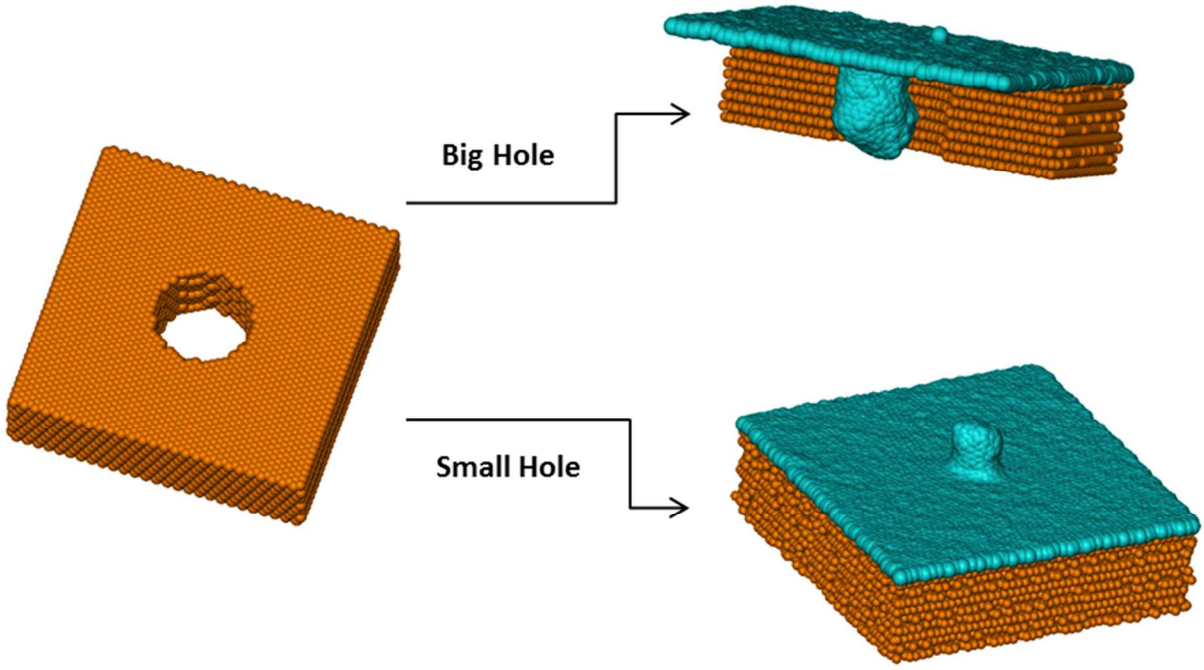

Two mechanisms of seamlessly C-C bonded junction formation:

i) CNT growth over the holes that are smaller than 3nm.

ii) CNT growth inside the holes that are larger than 3nm.

Journal Name

RSCPublishing

ARTICLE

Growth Mechanisms and Mechanical Properties of 3D Carbon Nanotube-Graphene Junctions: Molecular Dynamic Simulations

Cite this: DOI: 10.1039/xoxxoooooox

Received ooth January 2012,
Accepted ooth January 2012

DOI: 10.1039/xoxxoooooox

www.rsc.org/

Jianbing Niu[a], Mingtao Li[a], and Zhenhai Xia[a,b]*

Growth process of 3D junctions of carbon nanotube (CNT)-graphene on copper templates with nano-holes was simulated with classical molecular dynamic (MD) simulation. The CNT, graphene and their seamlessly C-C bonded junction can form simultaneously on the templates without catalysts. There are two mechanisms of the junction formation: i) CNT growth over the holes that are smaller than 3nm, and ii) CNT growth inside the holes that are larger than 3nm. Tensile strength of the as-growth C-C junctions as well as the junctions embedded with metal nanoparticles (catalysts) was determined via a quantum mechanics MD simulation method. Metal nanoparticles as catalysts remaining in the junctions significantly reduce the fracture strength and fracture energy, making them brittle and weak. Among the junctions, the seamlessly C-C bonded junctions show the highest tensile strength and fracture energy due to their unique structures. This work provides a theoretical base and a route for synthesizing high-quality single-layer CNT-graphene nanostructures.

1. Introduction

Carbon nanotube (CNT) and graphene, as one dimensional and two dimensional materials, attract extraordinary research interests in broad area, across materials science, physics, chemistry, medicine, biology etc. Recently, the 3D nanostructure - hybrid of graphene sheet and pillared single wall or multi-wall CNTs caught more attention in both experimental and theoretical fields.[1-6] Assembling these one dimensional CNT and two dimensional graphene with seamless CNT-graphene junctions can create 3D hybrid nanostructures with new functions while complementing their properties and retaining their advantage in maximum. For instance, the structure of graphene sheet and vertical single-wall or multi-wall CNTs was reported to possess broad application prospect such as energy storage,[7] thermal sinker [8, 9] and electronic devices.[10-11]

3D nanostructures were produced in laboratory in the presence of metal catalysts.[12-14] The growth of junction of 3D carbon nanotube-graphene was also simulated via quantum mechanical molecular dynamic method, providing specific theoretic foundations for the experimental effort to fabricate the new 3D structures.[15] However, most 3D nanostructures were fabricated with the aid of metal particle catalysts, in which the metal particles remain in the junction structure even after subsequent treatments. Therefore, understanding of mechanical properties and stability of the 3D nanostructures with metal particles is necessary for their applications. Simulation work has been done on mechanical property of large scale of pure C-C bonded CNT-graphene structure, [16-18] most of which, however, were focused on CNT density and lengths selected as the main variables, with the assumption of prefect junctions. Obviously, junctions are the key elements in the 3D structures and metal particles at the junctions would strongly affect the junction performance. Thus, the strength of junctions with metal particle would be of significance for the whole 3D nanostructure and needs more consideration.

To avoid the problem of catalysts remaining in the 3D CNT-graphene nanostructures, it is highly desirable to synthesize the nanostructures without catalysts. It has been shown that single-layer graphene can be grown on copper substrates.[19-25] In this paper, we proposed a new process based on copper templates to synthesize the 3D nanostructure without catalysts. The synthesizing process of single CNT-graphene junctions was simulated via molecular dynamic simulations. Furthermore, quantum mechanical molecular dynamic method was utilized to simulate the mechanical properties of as-grown C-C junctions as well as the junctions with metal nanoparticles embedded inside them.

2. Results and discussions

2.1 Formation of large-scale 3D CNT-graphene junctions

Journal Name

RSCPublishing

ARTICLE

The growth processes of graphene, CNT and their junctions on the Cu templates with different hole sizes (1-6 nm in diameter) were simulated using classical MD method. Generally, a single layer graphene forms quickly on the (111) surface of the Cu template, followed by the formation of a seamlessly C-C bonded CNT-graphene junction and the growth of CNT. Eventually, a 3D single-walled CNT-graphene nanostructure was formed and the architecture of 3D structure was determined by the template design.

It was found that there are two growth mechanisms for the junction formation, depending on the size of the hole. When the hole diameter is larger than 3 nm, after the formation of the graphene over the template surface (Fig. 1(a)), the newly formed graphene surrounding the hole curves down into the hole to form an embryo of CNT cap (Fig. 1(b)). With the feeding of carbon sources, the cap keeps growing into the hole to form a CNT (Fig. 1(c)). The detailed growing process can be seen in supplementary information (Video S1).

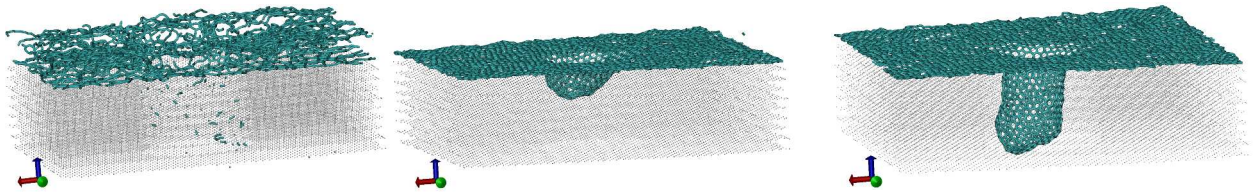

(a) (b) (c)

Fig. 1 (a) Carbon atoms deposited over the template surface; (b) formation of graphene and an embryo of CNT cap; (c) The CNT grown into the hole to form CNT-graphene junction.

When the hole diameter is smaller than 3nm, we observed an interesting CNT growing mechanism, as shown in Fig. 2. Instead of growing into the hole, the embryo of CNT grows upward over the hole to form CNT and junction as shown in Fig. 3. In the initial stage of growing, the template surface was first covered by randomly distributed carbon atoms (Fig. 2(b)), and then defective graphene formed from these carbon sources (Fig. 2(c)). In the initial stage, the graphene sheet has a hole as well at the Cu hole area due to lack of supporting. During relaxation it is generally sealed by C atoms, and a whole piece of graphene sheet formed. The extra C atoms diffuse on the graphene surface in single atom as well as in cluster (Fig. 2(c)). These carbon sources eventually move into the hole area and a CNT grows out of the graphene, as shown in Fig. 2(d). Since the CNT grows upward over the hole, this growth mode could simplify the post processing, providing a new route for synthesis of 3D CNT-graphene nanostructures with seamless C-C bonded junction without templating/catalyst. For example, the CNT-graphene layer could be simply peeled off the templetes and transferred to other substrates without damage the junction. To realize this process, the hole in the templates should be very small (e.g., < 3nm, as shown in the simulations).

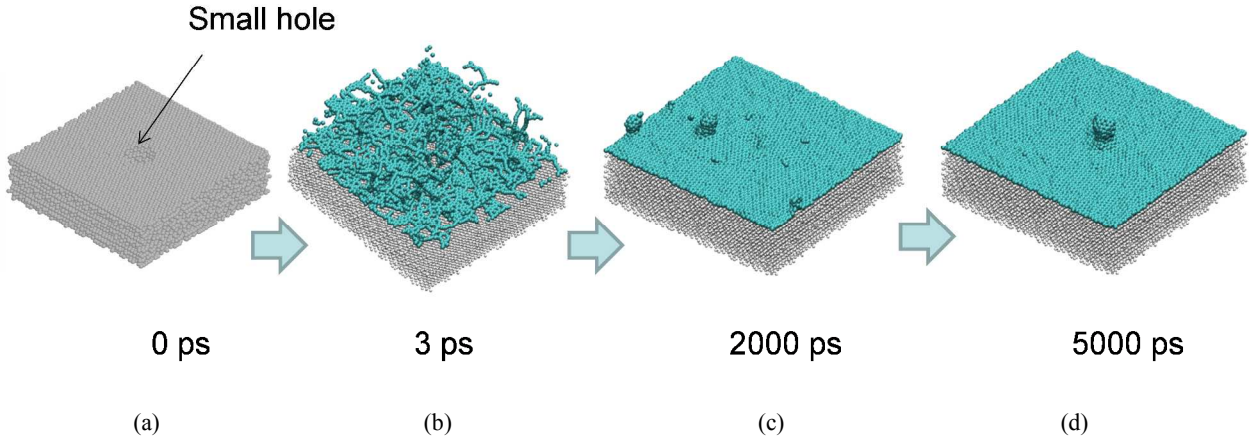

(a) (b) (c) (d)

Fig. 2 (a) Cu template with small hole (dimameter: 2 nm). (b) Template surface was first covered by randomly-distributed carbon atoms. (c) defective graphene formed from these carbon sources and covered the surface and the extra C atoms diffused on the graphene surface in single atom as well as in cluster, and (d) CNT growth out of the graphene after extra carbon atoms diffuse into the hole area.

Journal Name RSCPublishing

ARTICLE

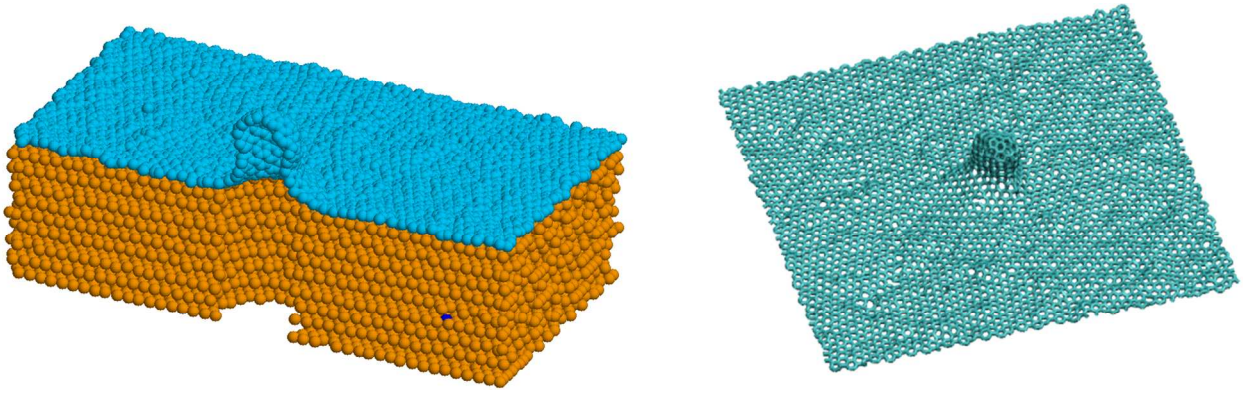

(a) (b)

Fig. 3 A CNT growing upward over the hole to form CNT-graphene junction. (a) Cross section of junction. (b) Top view of the junction after the template is removed.

We have studied the structural evolution of 3D nanostructures during their growth. Fig. 4(a) shows the number of atoms with different bond types for the nanostructure growing on Cu template with a 4 nm diameter hole. The number of sp^2 bonds increases rapidly at the initial stage and then reaches a plateau while the number of other type of bonds (sp^0 and sp^1) quickly reduces to a low level. There are almost no sp^3 bonds in the system mainly because the growing nanostructures consist of single-layer graphene, CNT and junctions. The small numbers of sp^0 and sp^1 bonds indicate defects and dangling bonds remaining due to incomplete relaxation. Obviously, the large number of sp^2 bonds indicates well-grown CNT, graphene and junction on template surface.

The number of polygons other than hexagons represents the quality of CNT and graphene in term of defects. Fig. 4(b) shows the number of polygons during the growth. While the number of pentagons and heptagons rapidly decreases, the number of hexagons rapidly increases. It is well known that pentagons and heptagons are typical defects in carbon materials and exist simultaneously in the form of Stone-Wales defects. As shown in Fig. 4(b), the population of hexagons is much larger than other types of carbon rings, suggesting that the CNT- graphene junctions are in high quality. The microstructure of the junctions was further examined after long time relaxation and both point and line defects were found in the structures, as reported in experiments.[45, 46] Fig. 5 shows a typical structure of CNT-graphene junctions. There are point defect (5577) and grain boundaries in the form of pentagons and heptagons distributed alternatively in graphene (Fig. 5(a)). Similar line defects are also found in CNT while these defects also exist in the transition region between graphene and CNT (Fig. 5(b)). The population of pentagons and heptagons in the junction area is larger than that in CNT and graphene. Thus, heptagons and pentagons are crucial for the formation of 3D CNT-graphene junctions.

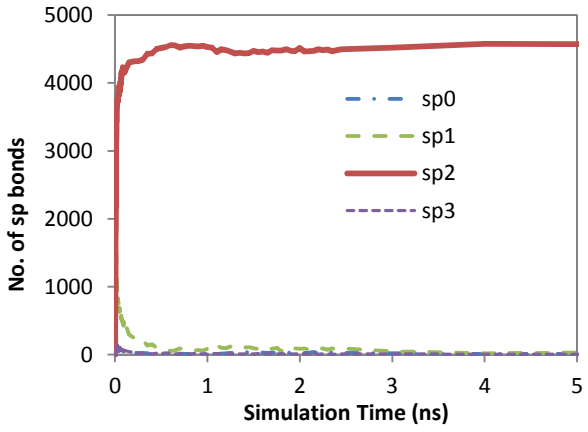

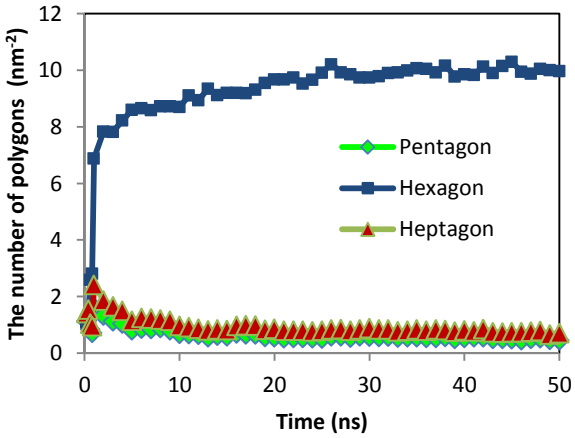

(a) (b)

Fig. 4 Structural evolution of the 3D nanostructure growing on Cu template with a 4 nm diameter hole: (a) The number of atoms with different bond types, and (b) the number of polygons during the growth.

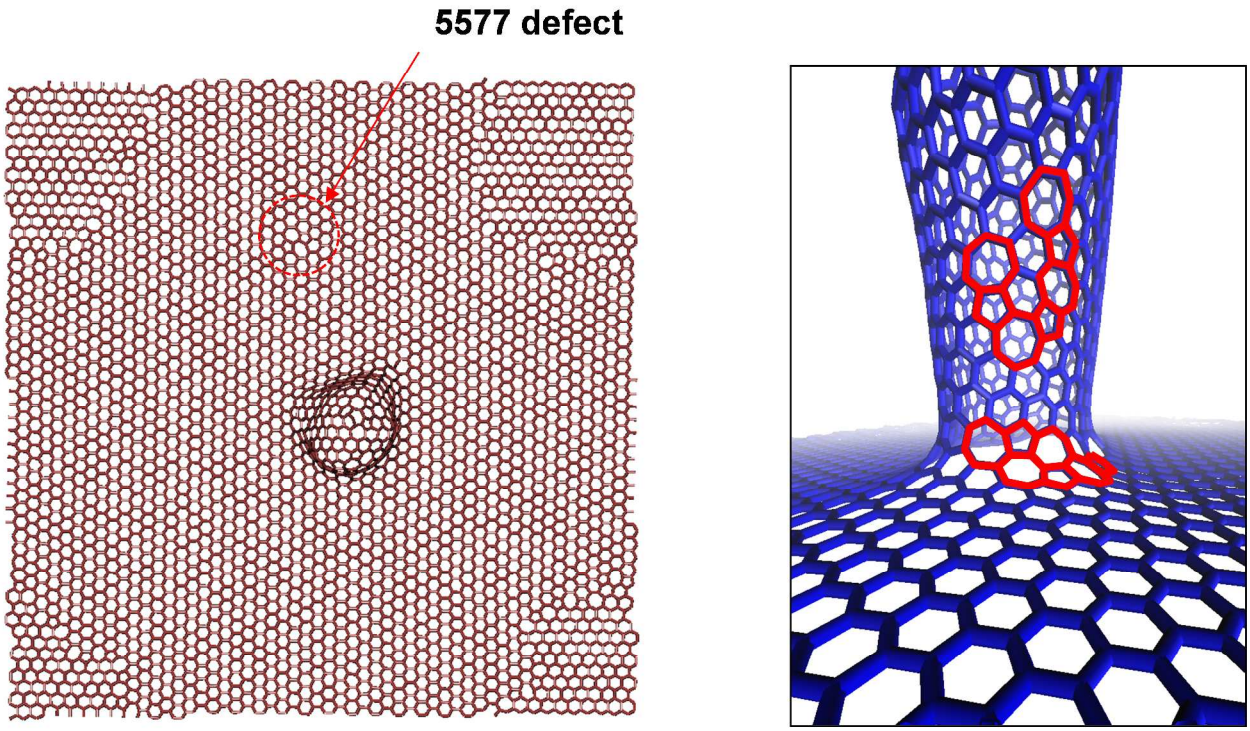

(a) (b)

Fig. 5 (a) single-layer CNT-graphene junction with point defect (5577) and grain boundaries in the form of pentagons and heptagons distributed alternatively in graphene, and (b) Similar line defects (highlighted in red) in CNT and the transition region between graphene and CNT.

2.2 Mechanical properties of different junctions

Carbon nanotubes with C-C sp^2 hybrids bonds are believed to be one of the strongest materials, with tensile strength of 85-118 GPa.[47] Pristine graphene, with similar C atoms arrangement to CNT, was reported to possess fracture strength of 100-126 GPa.[48] With such high strength, mechanical properties of the 3D nanostructure composed of graphene and vertical CNT will strongly depend on the quality of their junctions. It has been shown from the simulations[15, 49, 50] and experiments[13, 51, 52] that CNT-graphene junctions could be pure C-C covalent, metal-C bonds or the mixtures of them. Here, we calculated the tensile strength of the as-grown CNT-graphene junctions described in section 3.1, as well as those with embedded metal nanoparticles (remaining catalysts) as simulated in our previous work.[15]

Stress-strain curves of various junctions as well as pristine (5, 5) armchair CNTs are shown in Fig. 6. For the CNTs, the stress increases nearly linearly with increasing strain, but drops after reaching a maximum value that is defined as the tensile strength. From the stress-strain dependence, this behavior can be ascribed to the typical brittle failure mechanism, as simulated by others.[47, 53] In contrast, the pure C-C junction and the junctions with embedded Fe and Ni particles show relatively ductile fracture modes according to the stress-strain curves. For the covalent C-C junction, the ductile fracture stems from the compliant of graphene with out-of-plane deformation since graphene is fixed at its edge during loading. In the case of particle-embedded junctions, the ductile deformation can be attributed to the deformation of complaint graphene as well as the metallic particles.

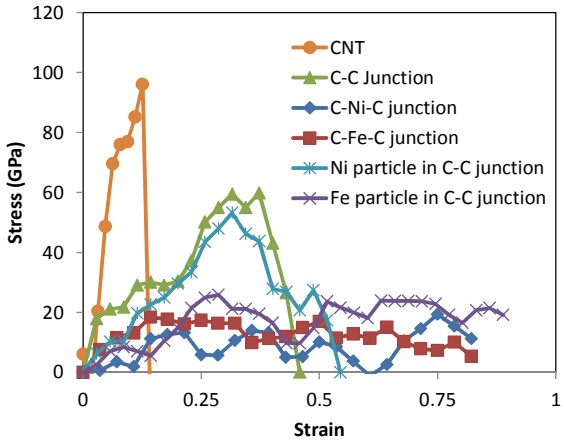

Fig. 6 Stress-strain curves for single-wall CNT, 3D C-C junction, junctions with Fe/Ni particles embedded between CNT and graphene (C-Fe-C and C-Ni-C junctions), and C-C junctions with Fe/Ni particles embedded in CNT.

Tensile strength of pure C-C junction is relatively lower than that of perfect CNTs. The lower strength is attributed to the existence of heptagons, pentagons, quadrangle at the junction area, which are considered as local defects. It was reported that for defective CNTs, the fracture strength reduces by ~9% for a Stone-Wales defect and ~26% for an atom vacancy.[26] Compared to pure C-C junction**,** tensile strength of metal-C junctions was further decreased by the metal particles embedded between CNT and graphene (Fig. 10(b)), even when metal particles are embedded within the junction and there are C-C bonds between CNT and graphene (Fig. 10(c)). When the metal particles are embedded between the CNT and graphene, the deformation of the junction obviously depends on the particle and metal-C bonds. For the junctions with metal particle embedded in the junction (Fig. 7(a)), the C-C bonds of the junction are weakened by the embedded particles. As a result, the C-C bonds prematurely break due to the existence of the nanoparticles, as shown in Fig. 7(b). After the C-C bonds at the junction are broken, the fracture mode is very similar to those junctions with metal particles embedded between the CNT and graphene, as shown in Fig. 7(c)-(d).

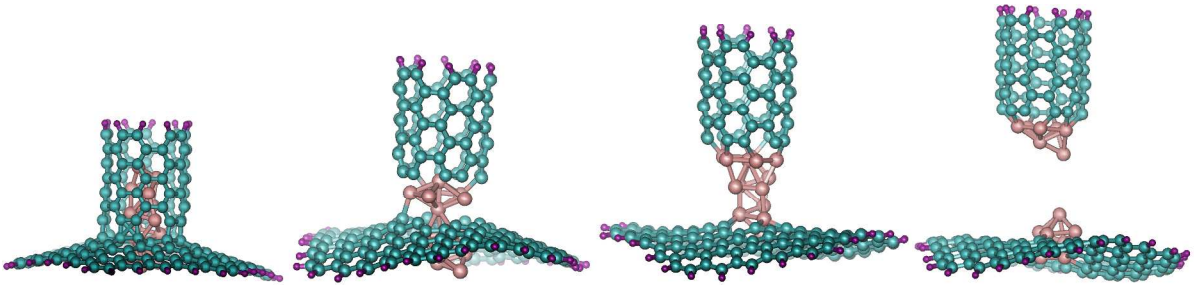

ε = 0% ε = 18.0% ε = 32.4% ε = 57.6%

(a) (b) (c) (d)

Fig. 7 Atomic configurations of fractured junctions with Fe particle embedded within the C-C bonded junctions: (a) Fe particle-embedded junctions, (b) junction with broken C-C bonds, (c) particle elongation, and (d) fractured junction. (ε represents tensile strain)

The fracture energy was also calculated from the area under the stress-strain (σ-ε) curves, shown in Fig. 8. The pure C-C bonded junctions have the highest fracture energy among the junctions. Metal particles can noticeably reduce fracture energy of the 3D junctions, depending on the particle embedding configurations. Fracture energy reduces by more than 50% as metal particles are embedded between the CNT and graphene, while it decreases slightly as metal particle is inside of junction for Fe and Ni particles. Obviously, the junction without metal particle has the highest tensile strength and ductility due to pure C-C covalent bonds. Thus, mechanical properties and deformation behavior of 3D nanostructure are strongly affected by remaining catalysts after junction growth, and it is necessary to remove the catalysts after the synthesis of the new 3D nanostructure or grow pure C-C bonded junctions without catalysts. As shown in Section 2.1, the high-quality single-layer

CNT-graphene junctions could be grown on Cu template without catalysts, providing an effective route to create 3D CNT-graphene nanostructures with seamlessly C-C bonded junctions.

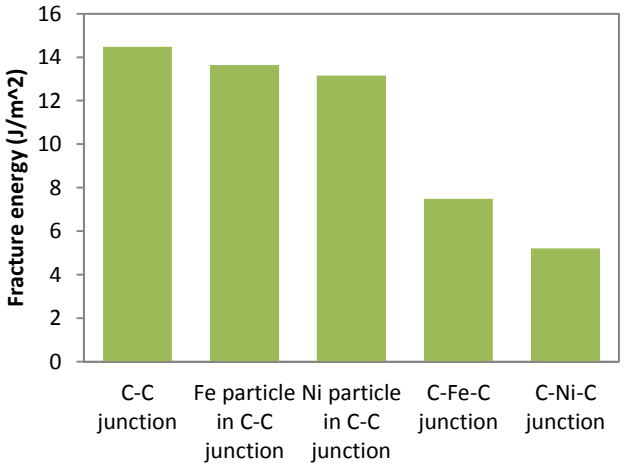

Fig. 8 Fracture energy of pure C-C junction and the junctions with embedded metal particles.

3. Computational Methodology

Templating growth of 3D CNT-graphene junctions: We proposed to deposit carbon sources on a copper template with hole on it, such that CNT could grow into the hole to form 3D CNT-graphene nanostructures. It has been reported that copper is an ideal substrate for the growth of single-layer graphene,[19-25] and single-wall CNT and single-layer graphene and their junctions could be fabricated with the copper template. To verify this idea, we used MD methods to simulate the growing process of the 3D nanostructures. The model system is composed of a copper substrate (template) and carbon sources. To generate the copper template, a single-crystal copper with a size of 12nmx 12nm x1.672nm was created with (111) on its surface. A hole of given diameter (d = 1~6 nm) was then drilled out of the center of the copper template, as shown in Fig. 9(a). Carbon sources are distributed over the template with an atom spacing of 0.3 nm. Periodic boundary conditions were applied in three directions to represent an infinite large system.

The MD algorithm was used here as implanted in the LAMMPS code to simulate the deposit of carbon atoms on the template by releasing the fixed carbon atoms discontinuously (Fig. 9(b)). The forces between Cu atoms were calculated using an EAM potential,[27-30] while the forces of the C atoms were computed using the second-generation reactive empirical bond-order potential (AIREBO).[31-34] These many-body potentials have been used to study the growth of carbon materials.[35] The interaction between C and Cu atoms were described by a Lannerd-Jones potential: $E=4\varepsilon\,[(\sigma/r)^{12}-(\sigma/r)^{6}]$ with r the distance between atoms, in which the parameters (ε = 0.02587 eV and σ=3.0825 Å) were used since experimental results has definitely shown that the interaction between the carbon atoms and copper atoms is weak.[36, 37] With a rescaling thermostat to control temperature (1073K), the equations of motion were integrated with a time step of 1.0 fs.

Fig. 9 (a) Copper template with (111) on surface and a hole in the center, and (b) deposit of carbon atoms placed at 0.5 nm above the Cu (111) surface for the growth of 3D CNT-graphene nanostructures.

Mechanical testing of the junctions: The tensile strength of pure C-C junctions and those with catalysts was calculated with quantum mechanical molecular dynamic software SCC-DFTB+ (self-consistent-charge Density Functional Tight Binding).[15,38-44] In the computation, Noose Hoover thermostat was utilized to perform all the activities of atoms with timestep of 1 fs. The tensile test was done at room temperature (300k). In laboratory, Fe and Ni are usually used as catalysts to grow carbon nanostructure; hence deformation of the junctions with different metal catalysts –Fe and Ni— was calculated. We tested three types of junctions: seamless C-C bond junctions (Fig. 10(a)), the junctions embedded with particles between CNT and graphene (C-Fe-C or C-Ni-C junctions; Fig. 10(b)) and the junctions with particle embedded inside CNT (Fig. 10(c)). All the models consists of a (5, 5) armchair CNT and single hexagonal graphene with an edge length of 1 nm. The graphene sheet was drilled out a hole of 0.65 nm, and CNT was placed above the nanoparticle and graphene. The outlining boundaries of CNT and graphene were saturated by hydrogen atoms. Nanoparticle size varies with different metals. The total number of the atoms in the simulation is around 250-290. For comparison, single CNT and as-grown C-C junctions made in the process simulations were also tested. The saturated H atoms on graphene was fixed during the simulations, and tensile test was performed by holding the H atoms and fist top ring of CNT, moving along CNT axial direction at a constant speed of 0.0125 nm/ps.

Journal Name RSCPublishing

ARTICLE

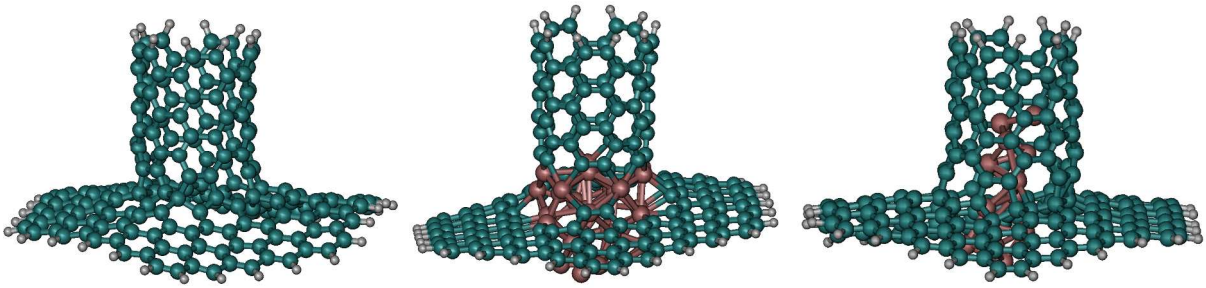

(a) (b) (c)

Fig. 10 Models for tensile testing of the junctions: (a) A pure C-C bonded junction, (b) A junction with Fe particle between CNT and graphene, and (c) A junction with Fe particle embedded in it. (Green represents C atoms, white is referred to H atoms; and pink represents Fe atoms)

4. Conclusions

Growth processes of 3D CNT-graphene junction on Cu templates were simulated via classical MD simulations. There are two growing mechanisms depending on the size of template holes: i) CNT growth over small hole, and ii) CNT growth inside large hole. Line and point defects were found in the grown CNT, graphene and junctions. Pentagons and heptagons play an important role in the junction growth especially at the transition region of CNT and graphene. The seamless C-C junction growth mechanisms found in this study provide a theoretic foundation for growth of 3D nanostructures without any catalysts. Tensile tests of different types of junctions in 3D nanotube – graphene nanostructures were simulated via quantum mechanical molecular dynamic method. The simulations show that the covalently C-C bonded junctions possess the highest fracture strength and fracture energy. The metal nanoparticles embedded in the junctions between the CNT and graphene significantly reduce the fracture strength and energy. Even when the metal particles are embedded inside junction, the C-C bonded junctions are weakened by the particles. Our simulations show that it possible to synthesize high-quality 3D CNT-graphene nanostructures using templating methods without catalysts.

Acknowledgements

We acknowledge support by Air Force Office of Scientific Research (AFOSR) MURI program (FA9550-12-1-0037) and National Science Foundation (NSF) CMMI program (CMMI-1212259, CMMI-1266319).

Notes and references

[a]Department of Materials Science and Engineering, University of North Texas, Denton, TX 76203, USA

[b]Department of Chemistry, University of North Texas, Denton, TX 76203, USA

*Corresponding author: Email: Zhenhai.xia@unt.edu, Tel: 940-369-5805, Fax: 940-565-4824

1. D. Yu and L. Dai, *J. Phys. Chem. Lett.*, 2010, **1**, 467–470.
2. S. Bae, K. Karthikeyan, Y. Lee and II-K. Oh, *CARBON*, 2013, **64**, 52 –536.
3. C. Kang, R. Baskaran, J. Hwang, B. Ku and W. Choi, *CARBON*, 2014, **68**, 493 –500.
4. Z. Fan, J. Yan, L. Zhi, Q. Zhang, T. Wei , J. Feng, M. Zhang, W. Qian and F. Wei, Adv. Mater., 2010, 22, 3723–3728.
5. G. C. Loh, E. H. T. Teo and B. K. Tay, *J. Appl. Phys.*, 2011,**110**, 083502.
6. R. P. Wesotowski and A. P. Terzyk, *Phys. Chem. Chem. Phys.,* 2011, **13**, 17027–17029.
7. G. K. Dimitrakakis, E. Tylianakis and G. E. Froudakis, *Nano Lett*, 2008, **8**, 3166–3170.
8. V. Varshney, S. S. Patnaik, A. K. Roy, G. Froudakis and B. L. Farmer, *ACS NANO,* 2010, **4**, 1153–1161.
9. L. Xu, N. Wei, Y. Zheng, Z. Fan, H. Wang and J. Zheng, *J. Mater. Chem.,* 2012, **22**, 1435–1444.
10. F. Du, D. Yu, L. Dai, S. Ganguli, V. Varshney and A. K. Roy, *Chem. Mater.,* 2011, **23**, 4810–4816.
11. Y. Kim, K. Kumar, F. T. Fisher and E. Yang, *Nanotechnology,* 2012, **23**, 015301.
12. J. Lin, C. Zhang, Z. Yan, Y. Zhu, Z. Peng, R. H. Hauge, D. Natelson and James M. Tour, *Nano Lett*, 2013, **13**, 72−78.
13. M. Zhao, X. Liu, Q. Zhang, G. Tian, J. Huang, W. Zhu and F. Wei, *ACS NANO,* 2012, **6**, 10759–10769.
14. J. Wen, Y. Li and W. Yang, *Vacuum*, 2014, **101**, 271-274.
15. J. Niu, M. Li, W. Choi, L. Dai and Z. Xia, *CARBON*, 2014, **67**, 627 –634.
16. S. Sihn, V. Varshney, A. K. Roy and B. L. Farmer, *CARBON,* 2012, **50**, 603–611.

17. S. Sihn, V. Varshney and A. K. Roy, 51st AIAA/ASME/ASCE/AHS/ASC Structures, Structural Dynamics, and Materials Conference
18th 12 - 15 April 2010, Orlando, Florida.
18. F. D. Novaes, R. Rurali and P. Ordejon, *ACS NANO*, 2010, **4**, 7596–7602.
19. X. Li, W. Cai, L. Colombo and R. S. Ruoff, *Nano Lett.,* 2009, **9**, 4268-4272.
20. X. Li, W. Cai, J. An, S. Kim, J. Nah, D. Yang, R. Piner, A. Velamakanni, I. Jung, E. Tutuc, S. K. Banerjee, L. Colombo and R. S. Ruoff, *Science,* 2009, **324**, 1312-1314.
21. J. D. Wood, S. W. Schmucker, A. S. Lyons, E. Pop and J. W. Lyding, *Nano Lett.,* 2011, **11**, 4547–4554.
22. Z. Sun, Z. Yan, J. Yao, E. Beitler, Y. Zhu and James M. Tour, *Nature,* 2010, **468**, 549-552.
23. L. Gao, J. R. Guest and N. P. Guisinger, *Nano Lett.,* 2010, **10**, 3512–3516.
24. J. M. Wofford, S. Nie, K. F. McCarty, N. C. Bartelt and O. D. Dubon, *Nano Lett.,* 2010, **10**, 4890–4896.
25. X. Li, C. W. Magnuson, A. Venugopal, R. M. Tromp, J. B. Hannon, E. M. Vogel, L. Colombo and R. S. Ruoff, *J. Am. Chem. Soc.,* 2011, **133**, 2816–2819.
26. S. L. Mielke, D. Troya, S. Zhang, J. Li, S. Xiao, R. Car, R. S. Ruoff, G. C. Schatz and T. Belytschko*, Chemical Physics Letters,* 2004, **390**, 413–420.
27. A. F. Voter, Los Alamos Unclassified Technical Report No. LA-UR-93-3901.
28. S. J. Zhou, D. M. Beazley, P. S. Lomdahl and B. L. Holian, *PRL,* 1996, **78**, 479-482.
29. C. L. Liu, J. M. Cohen, J. B. Adams and A. F. Voter, *Surface Science,* 1991, **253**,334-344.
30. S. M. Foiles, M. I. Baskes and M. S. Daw, *Phys. Rev. B,* 1986, **33**, 7983.
31. D. W. Brenner, O. A. Shenderova, J. A. Harrison, S. J. Stuart, B. Ni and S. B. Sinnott, *J. Phys.: Condens. Matter.,* 2002, **14**, 783–802.
32. D. W. Brenner, *Phys. Rev. B,* 1990, **42**, 9459-9471.
33. J. A. Harrison, C. T. White, R. J. Colton and D. W. Brenner, *Phys. Rev. B,*1992, **46**, 9700-9708.
34. D. W. Brenner, D. H. Robertson, ML. Elert and C. T. White, *Phys Rev Lett*, 1993, **70**, 2174-2177.
35. S. Banerjee, S. Naha and I. K. Puri, *Appl. Phys. Lett.,* 2008, **92**, 233121.
36. A. L. Va´zquez de Parga, F. Calleja, B. Borca, M. C. G. Passeggi, Jr., J. J. Hinarejos, F. Guinea, and R. Miranda, *PRL,* 2008,**100**, 056807.
37. P. Sutter, J. T. Sadowski and E. Sutter, *Phys. Rev*. B, 2009, **80**, 245411.
38. http://www.dftb.org/
39. A. J. Page, Y. Ohta, S. Irle and K. Morokuma, *Acc. Chem. Res.* 2010, **43**, 1375-1385.
40. Y. Ohta, Y. Okamoto, S. Irle and K. Morokuma, *CARBON,* 2009, **47**, 1270–1275.
41. Y. Ohta, Y. Okamoto, A. J. Page, S. Irle and K. Morokuma, *ACS NANO,* 2009, **3**, 3413–3420.
42. A. J. Page, H. Yamane, Y. Ohta, S. Irle and K. Morokuma, *J. Am. Chem. Soc.* 2010, **132**, 15699–15707.
43. A. J. Page, S. Minami, Y. Ohta, S. Irle and K. Morokuma, *CARBON,* 2010, **48**, 3014–3026.
44. A. J. Page, S. Irle and K. Morokuma, *J. Phys. Chem. C,* 2010, **114**, 8206–8211.
45. J. C. Meyer, A. Chuvilin, G. Algara-Siller, J. Biskupek and U. Kaiser, *Nano Lett.,* 2009, **9**, 2683-2689.
46. J. C. Meyer, C. Kisielowski, R. Erni, M. D. Rossell, M. F. Crommie, and A. Zettl. *Nano Lett.*, 2008, **8**, 3582-3586.
47. T. Belytschko, S. P. Xiao, G. C. Schatz and R. Ruoff, *Phys. Rev. B,* 2002, **65**, 235430.
48. M. C. Wang, C. Yan, L. Ma, N. Hu and M.W. Chen, *Computational Materials Science,* 2012, **54**, 236–239.
49. J. Park and V. Prakash, *J. Mater. Res.,* 2013, **28**, 940-951.
50. D. Baowan, B. J. Cox and J. M. Hill. *Carbon,* 2007, **45**, 2972–2980.
51. Z. Yan, L. Ma, Y. Zhu, I. Lahiri, Z. Liu, M. G. Hahm, S. Yang, C. Xiang, W. Lu, Z. Peng, Z. Sun, J. Lou, W. Choi, P. M. Ajayan and J. M. Tour, *Acs Nano*, 2013, **7**, 58-64.
52. Y. Zhu, L. Li, C. Zhang, G. Casillas, Z. Sun, Z. Yan, G. Ruan, Z. Peng, A. R. O. Raji, C. Kittrell, R. H. Hauge and J. M. Tour, *Nature commu.,* 2012, **3**, 1225.
53. M. B. Nardelli, B. I. Yakobson and J. Bernholc, *PRL.* 1998, **81**, 4656-4659.

